



Choosing wavelet methods for otolith contour studies

Joana Vasconcelos · José Luís Otero-Ferrer ·
Antoni Lombarte · Alba Jurado-Ruzafa ·
Amalia Manjabacas · Víctor M. Tuset

Received: 25 March 2024 / Accepted: 15 September 2024
© The Author(s) 2024

Abstract Otolith shape analysis has been extensively employed to distinguish stocks and populations of marine fish species. While the majority of studies have employed Elliptic Fourier descriptors (EFD) for this purpose, an alternative approach was introduced in 2005 founded on the Wavelet Transform, using the à trous multiscale signal representation with a B3-Spline function. This approach not only improved the biological and mathematical interpretation but

also empowered the user to select a more suitable level based on the contour complexity. Recently, the global adoption of the mathematical R environment enabled the creation of a freely accessible package called *shapeR* for otolith shape analysis using Daubechies least-asymmetric wavelet. Nevertheless, we have pinpointed certain inconsistencies in this package concerning the biological implications of its results and a deviation from the original application philosophy. To illustrate these inconsistencies, we conducted a study aiming to differentiate populations and morphotypes of the blue jack mackerel, *Trachurus picturatus*, from the Canary Islands and

Supplementary Information The online version contains supplementary material available at <https://doi.org/10.1007/s11160-024-09896-6>.

J. Vasconcelos
BIOCON, IU-ECOQUA, Universidad de Las Palmas de Gran Canaria, Edificio de Ciencias Básicas, Campus Universitario de Tafira, 35017 Las Palmas, Gran Canaria, Spain

J. Vasconcelos (✉)
MARE - Marine and Environmental Sciences Centre/
ARNET - Aquatic Research Network, Agência Regional para o Desenvolvimento da Investigação Tecnológica e Inovação (ARDITI), Edif. Madeira Tecnopolo, Piso 2, Caminho da Penteada, 9020–105 Funchal, Madeira, Portugal
e-mail: joanapatricia.reis@ulpgc.es

J. L. Otero-Ferrer
Biostattech, Advice, Training and Innovation in Biostatistics (Ltd.), Edificio Emprendia, Campus Sur s/n, Cruce Avda. Maestro Mateo- Carretera San Lorenzo, 15782 Santiago de Compostela, Spain
e-mail: joseluis.oteroferre@gmail.com

A. Lombarte · A. Manjabacas
Department de Recursos Marins Renovables, Institut de Ciències del Mar (ICM-CSIC), Passeig Marítim de la Barceloneta, 3749, 08003 Barcelona, Catalonia, Spain
e-mail: toni@icm.csic.es

A. Manjabacas
e-mail: manjabacas@icm.csic.es

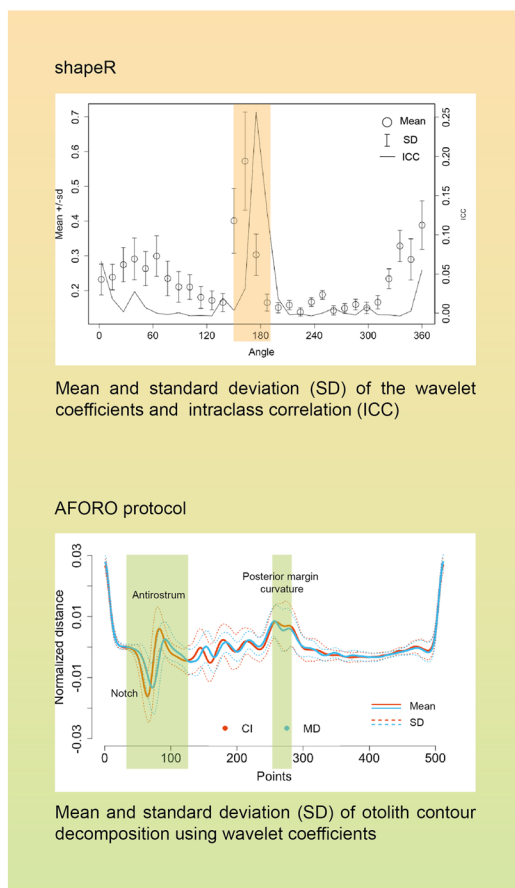
A. Jurado-Ruzafa
Centro Oceanográfico de Canarias, Instituto Español de Oceanografía (IEO, CSIC), Calle Farola del Mar 22, 38180 Santa Cruz de Tenerife, Canary Island, Spain
e-mail: alba.jurado@ieo.csic.es

V. M. Tuset
Instituto de Oceanografía y Cambio Global (IOCAG), Universidad de Las Palmas de Gran Canaria, Parque Científico Tecnológico Marino de Taliarte, s/n, 35214 Telde, Canary Islands, Spain
e-mail: vtuset@ulpgc.es

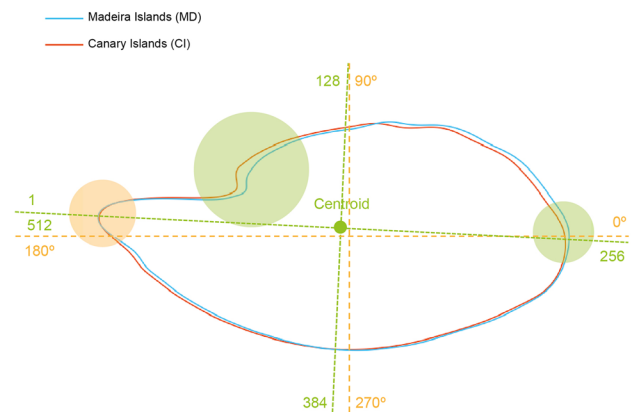
Madeira. We employed both *shapeR* package and our original method in the comparison. Furthermore, we evaluated the performance of different parametric and non-parametric classification algorithms using wavelet coefficients obtained from both methodologies. This study has shown that both methods are suitable for population identification, achieving high classification accuracy. However, some inconsistencies were observed between the graphical representation

of the intraclass correlation plot and the mean otolith contour reconstruction using the *shapeR* package. AFORO demonstrates a particular strength in capturing morphological changes, allowing for better identification of contour shape variations along the wavelet signal. Additionally, both methods identified the same number of morphotypes within the overall sample, albeit with differing proportions.

Graphical abstract



Choosing Wavelet Methods for Otolith Contour Studies



Mean otolith shape based on wavelet reconstruction for *Trachurus picturatus*. Degrees for **shapeR** and 512 points for **AFORO protocol**.

Keywords Otolith shape analysis · Wavelets · *shapeR* · AFORO · *Trachurus picturatus* · North and Central East Atlantic

Introduction

Ensuring the responsible management of fisheries resources requires the ability to distinguish between fish stocks and to delimit their boundaries and connectivity for adequate assessment and management of marine resources (Begg et al. 1999; Vasconcelos et al. 2021). There are different techniques for this purpose as, for example, the analysis of otolith's microchemistry and shape, which are calcium carbonate structures found in the inner ear of bony fishes, commonly used as biological markers (e.g., Abaunza et al. 2008; Cadrin et al. 2013; Marengo et al. 2017; Smoliński et al. 2020). Focusing on otolith shape, the contour recognition has traditionally relied on Fourier descriptors, with the most common method being Elliptic Fourier analysis (EFA). This method captures overall shape variability by combining harmonics, which illustrate the contribution of signals of specific frequencies to the overall shape (e.g., Kuhl and Giardina 1982; Messieh et al. 1989; Bird et al. 1986; Campana and Casselman 1993; Friedland and Reddin 1994; Tracey et al. 2006; Stransky et al. 2008). However, its ability to pinpoint intricate details or subtle features on the contour is limited and requires many harmonics (Parisi-Baradad et al. 2005). This can pose challenges in achieving high success rates in classification, particularly depending on the variability of contour irregularities (e.g., Lombarte and Morales-Nin 1995; Tuset et al. 2003; Burke et al. 2008; Neves et al. 2021). To address this issue, alternative approaches have been proposed, such as curvature-based descriptors (Begg et al. 2005; Parisi-Baradad et al. 2005), shape geodesics (Nasreddine et al. 2009), mirroring techniques (Harbitz and Albert 2015), the Shapelet transform method (Lines et al. 2012; Mapp et al. 2013; Hills et al. 2014), and wavelets (Parisi-Baradad et al. 2005, 2010; Piera et al. 2005; Lombarte et al. 2006; Libungan et al. 2015). In particular, wavelets have the ability to precisely describe specific morphological features linked to biologically significant points, such as the *rostrum* and *antirostrum*, as well as irregularities along the contour (Parisi-Baradad et al. 2005). This attribute has attracted heightened attention and has generated a substantial body of research.

The commercial software Age&Shape (Infaimon SL©, Barcelona, Spain) was developed by teams from the Universitat Politècnica de Catalunya

(UPC), Institut Mediterrani d'Estudis Avançats (IMEDEA-CSIC) and Institut de Ciències del Mar (ICM-CSIC). It was designed to analyze the contour of hard structures using wavelet function, as well as other options such as Elliptic Fourier and Fast Fourier Transform. The wavelet function employed, the B3 spline wavelet, is a non-orthogonal filter with a symmetric shape and excellent regularity properties, making it well-suited for analyzing smooth signals (Parisi-Baradad et al. 2010). Additionally, the à trous algorithm used in our approach is a redundant transform that computes wavelet coefficients at each scale by convolving the signal with the dilated wavelet filter. Over time and through extensive experience with various species, the usefulness of DWT and scale selection has become increasingly evident in studies on interspecific diversity (Sadighzadeh et al. 2012; Tuset et al. 2015; Lombarte et al. 2018), intraspecific phenotypic variability (Vasconcelos et al. 2021), and stock delineation (Sadighzadeh et al. 2014; Tuset et al. 2019). Despite the software's swift discontinuation, this methodology remains accessible online through the AFORO website (<http://aforo.cmima.csic.es/>), while an R-based version of Age&Shape is currently in development. Concurrently with these developments, Libungan and Pálsson (Libungan and Pálsson 2015) launched the open-source *shapeR* package for the R environment (R Core Team 2023). This package presents a well-designed workflow and offers a user-friendly suite of functions aimed at streamlining tasks such as extracting otolith outlines from images and visualizing average shapes. It also facilitates contour analysis through methods like EFA and wavelets. The *shapeR* package uses Daubechies wavelets, which are orthogonal filters with compact support and a varying number of vanishing moments (Kumar and Foufoula-Georgiou 1994), making them useful for analyzing signals with singularities and discontinuities. Unlike the à trous algorithm used in AFORO, the Mallat algorithm implemented in *shapeR* employs non-redundant Daubechies wavelet transform, using a pyramidal scheme to decompose the signal into approximation and detail coefficients at different scales. This package has been widely adopted in numerous studies to infer intraspecific variation, spatial structure of fish populations, and ecomorphological patterns using EFA (Soeth et al. 2019; Neves et al. 2021),

DWT (Christensen et al. 2018; Sadeghi et al. 2020; Schroeder et al. 2022) or both (Libungan et al. 2015; Vaux et al. 2019; Jónsson et al. 2021; Morawicki et al. 2022; Deville et al. 2023).

Our study focuses on comparing the outputs of *shapeR* with the methodology developed by the AFORO for the identification of populations and phenotypes. The blue jack mackerel, *Trachurus picturatus*, was used as case study. The present work aims to: (1) morphologically interpret the plots depicting the variability observed in the otolith contour; (2) compare the level of classification success between populations (average phenotype); and (3) determine the degree of phenotypic differentiation when considering all individuals as a metapopulation.

Methods

Otolith collection

Between 2005 and 2018, a total of 550 blue jack mackerel specimens, *Trachurus picturatus* (Table S1) were collected from the waters adjacent to the Canary Islands (CI) and Madeira (MD) (the geographical areas are illustrated in the map presented in Vasconcelos et al. (2021)). Specimens from the Canary Islands were kept frozen at -20°C until laboratory processing, while those from Madeira were examined fresh. The total length (TL) of each specimen was measured to the nearest 0.1 cm, and a correction factor (Jurado-Ruzafa and García Santamaría 2013) was applied to the Canary Islands samples to adjust for size loss due to freezing. Only individuals with TL > 17 cm (Jurado-Ruzafa and García Santamaría 2013; Vasconcelos et al. 2018, 2021) were included in the study to minimize ontogenetic effects on phenotypic variation (Lombarte and Castellón 1991). *Sagittae* otoliths were extracted, cleaned, and stored dry in labelled Eppendorf tubes for morphological analyses.

Photo acquisition

The intact left otoliths were positioned on a dark background, with the *sulcus acusticus* facing downward and the *rostrum* to the left on the horizontal plane to minimize errors during the normalization and digitization processes. Although it is commonly

recommended to capture photographs of otoliths with the *sulcus acusticus* facing upward and the *rostrum* to the right (Tuset et al. 2008), the images in this study were specifically taken for age determination purposes. High-contrast digital images of each otolith were obtained using digital cameras coupled to stereomicroscopes. The cameras were adjusted to a magnification of 10x using imaging software such as NIS-Elements F@imaging software (Instituto Español de Oceanografía, IEO, Canary Islands) and the Leica Application Suite software (LAS version 4.5, Leica Microsystems, Wetzlar, Germany, www.leica-microsystems.com) (Direção Regional das Pescas, Madeira). Otolith lengths (OL) were measured with a precision of 0.01 mm using ImageJ (Schneider et al. 2012) and Leica Application Suite X Core. To correct the orientation during the digitization process in the *shapeR* R package (Libungan and Pálsson 2022), we used Photopea, an online image editing tool developed by Kutsir (2022).

shapeR R package

Wavelet coefficients were derived using the *shapeR* R package, following the protocol outlined by Libungan and Pálsson (2015), as described below. The outlines were automatically extracted from the otolith images by applying a threshold of 0.2 to distinguish the otoliths from the dark background. To ensure accuracy and consistency, the extracted outlines of each otolith were superimposed onto the original images. Upon detecting errors in the outline representation, the otolith images underwent conversion to black and white using Photopea (Kutsir 2022), followed by subsequent re-evaluation. Despite the original photos featuring a black background, it was essential to modify the color of several otoliths to white to facilitate the analysis, especially at lower threshold levels (Morales et al. 2023). We opted not to smooth the outlines of the otoliths to avoid excessive reduction of pixel noise in the photos. After capturing all the outlines, the wavelet coefficients were extracted. To obtain polar coordinates, a horizontal radial axis was drawn from the centroid of the otolith towards the right side of the image, corresponding to the 0° angle of the otolith outline, where the posterior part of the otolith is located. Equally spaced radii were then generated counterclockwise from this starting point, progressing until the 360° angle. These radii underwent

transformation into wavelet coefficients through the application of a discrete wavelet transform (Nason 2012). Specifically, the Daubechies least-asymmetric wavelet (Gençay et al. 2001) was applied, resulting in a total of 64 wavelet coefficients obtained from five wavelet levels. To account for the effects of otolith size (Stransky and MacLellan 2005), the function *stdCoefs* was applied. Coefficients that showed a significant interaction ($p < 0.05$) between variables were removed. For a more precise assessment of the differences between populations, the intraclass correlation (ICC) was calculated. The ICC serves as a metric indicating the proportion of variation present among different groups. Variations in contour shape among populations were examined with a Canonical Analysis of Principal Coordinates (CAP) (Anderson and Willis 2003) using the *vegan* R package (Oksanen et al. 2022). To evaluate the significance of constraints, the ANOVA-like permutation test was performed (Oksanen et al. 2022).

AFORO protocol in R

A total of 512 equidistant Cartesian coordinates were extracted from each orthogonal projection of the otolith, with the *rostrum* as the origin (Parisi-Baradad et al. 2005, 2010; Lombarte et al. 2006). From each contour, nine wavelets were derived based on the degree of otolith detail. Following previous studies on identification of stocks and phenotypes, the 4th wavelet was specifically chosen since this level provides sufficient detail to accurately define the otolith silhouette (Sadighzadeh et al. 2014; Tuset et al. 2019; Vasconcelos et al. 2021). To retain information of wavelet transform without any loss, a principal component analysis (PCA) was performed on the variance covariance matrix (Sadighzadeh et al. 2012; Tuset et al. 2019, 2021). The percentage of total variation explained by the eigenvectors was plotted against the proportion of variance expected under the “broken stick model” to identify significant eigenvectors (Gauldie and Crampton 2002). As allometry may contribute to intraspecific differences, linear regressions were assessed between otolith size and the principal components (Stransky and MacLellan 2005). Subsequently, the effect of otolith size was eliminated by constructing a new PCA matrix using the residuals from the common within-group slopes of the linear regressions of each component on otolith size.

The significant total variation was assessed using permutational multivariate analysis of variance (PERMANOVA; (Anderson 2001)) with 999 permutations using the Manhattan distance and Bonferroni correction for post-hoc pairwise multiple comparisons.

Accuracy of classification

For comparing populations using both methods, three distinct non-parametric classification algorithms - Multilayer Perceptron (MLP), Support Vector Machine (SVM), and K-nearest Neighbors (KNN), along with an alternative version of Linear Discriminant Analysis (LDA) were chosen (Youssef et al. 2016; Smoliński et al. 2020; Tuset et al. 2021). We performed a repeated (‘repeatedcv’) cross-validation with 4 folds and 100 repetitions to evaluate the performance of our machine learning model. The models were constructed using scaled and centred predictor variables. The optimal hyperparameters (hidden units) were determined during preliminary tuning (Supplementary Figures 1 and 2). Confusion matrices (error matrices) were created, and classification accuracy, representing the percentage of fish correctly assigned to their actual class, was computed as a metric for evaluating classifier quality. The *caret* R package (Kuhn 2008) was employed for the classification tasks.

Identifying phenotypes

To explore a range of possible cluster numbers for morphotype determination, we conducted a hierarchical cluster analysis using four different methods (ward, complete, average, and single) with the *hclust* function from the *stats* R package (R Core Team 2023). This analysis was based on distance matrices computed from CAP scores for the *shapeR* analysis and PCA results from the AFORO protocol in R. The ward method was chosen as the optimal approach to determine the minimum and maximum number of clusters within the evaluated range. In our study, a minimum of four clusters was identified as optimal (Supplementary Figures 3 and 4). To determine the optimal number of phenotypes or morphotypes in the entire sample, we conducted a cluster analysis using the *clValid* R package (Brock et al. 2008). This package integrates a single function that facilitates the simultaneous comparison of various

clustering algorithms, including clara, diana, hierarchical, k-means, model, pam, and sota, across different numbers of clusters (Brock et al. 2008). *cValid* also reports validation measures for clustering results. This feature streamlines the evaluation and comparison of multiple clustering approaches within a single analysis. For the cluster analysis, we used the shape coefficients obtained from *shapeR* and the new PC matrix obtained through the AFORO. The analysis employed the Manhattan distance as the similarity measure and the Ward method for hierarchical clustering. This approach enhanced the visual separation of phenotypes, facilitating the determination of the potential range for the minimum and maximum number of clusters. To assess the quality and stability of the obtained clusters, we employed two validation measures: “internal” and “stability”. The non-parametric Kruskal-Wallis rank sum test (KW test) was used to compare mean density among phenotypes on the first principal coordinate of CAP (*shapeR*) and the first component of PCA (AFORO) (O’Dea et al. 2019), owing to its suitability for analyzing phenotypic variations associated with environmental factors such as temperature (Vasconcelos et al. 2021). The post-hoc Pairwise Wilcoxon rank sum test (WRS test) was applied to calculate pairwise comparisons across phenotypes with corrections for multiple testing. The method selected for adjusting p values was the “bonferroni”. The selection of this first CAP and PC was based on the highest variability explained (Supplementary Figure 5).

Results

Exploring the contour’s variability

The quality of the wavelet reconstruction using *shapeR* was assessed, and the 5th wavelet was chosen for subsequent analyses as it achieves the 98.5% accuracy required for the reconstruction. The wavelet coefficients were standardized according to otolith length. The average otolith shape showed differences among populations in the *antirostrum* and the dorsal zone (Fig. 1A). In particular, otoliths from the Canary Islands (CI) exhibit more pronounced *antirostrum* and a more developed anterior-dorsal region, whereas those from Madeira (MD) were wider in the dorsal-ventral region. However, in contrast to the average

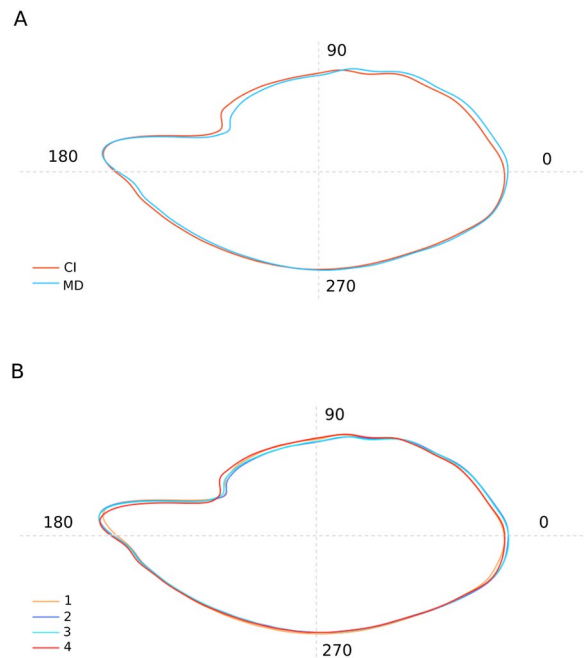


Fig. 1 Mean otolith shape reconstructed using wavelet analysis for the average phenotype and four morphotypes (M1, M2, M3, and M4) identified in *Trachurus picturatus* samples from the north and central eastern Atlantic Ocean, specifically from the Canary (CI) and Madeira (MD) archipelagos. This analysis was conducted using the *shapeR* R package

otolith shape (Fig. 1A), the examination of the intra-class correlation (ICC) and the mean and standard deviation (Fig. 2A) reveals minimal variability along the entire contour, except for the region spanning angles 160–190°, corresponding to the peak of the *rostrum*. Other secondary zones also exhibited variations to a lesser extent, ranging between 340–360°, representing the ventral-posterior area. The analysis revealed a significant distinction between the otolith shape of the Canary Islands and Madeira populations along the first discriminating axis (CAP1, see Fig. 3A). This axis accounted for 100% of the observed variation. The populations from the CI and MD showed significant differences in the otolith shape (ANOVA: pseudo-F = 38.469, df = 1, $p = 0.001$).

The PCA analysis obtained from AFORO revealed that the first 26 principal components explained 77.31% of the total variance, indicating that variance attributable to chance alone is distributed across many dimensions (Supplementary

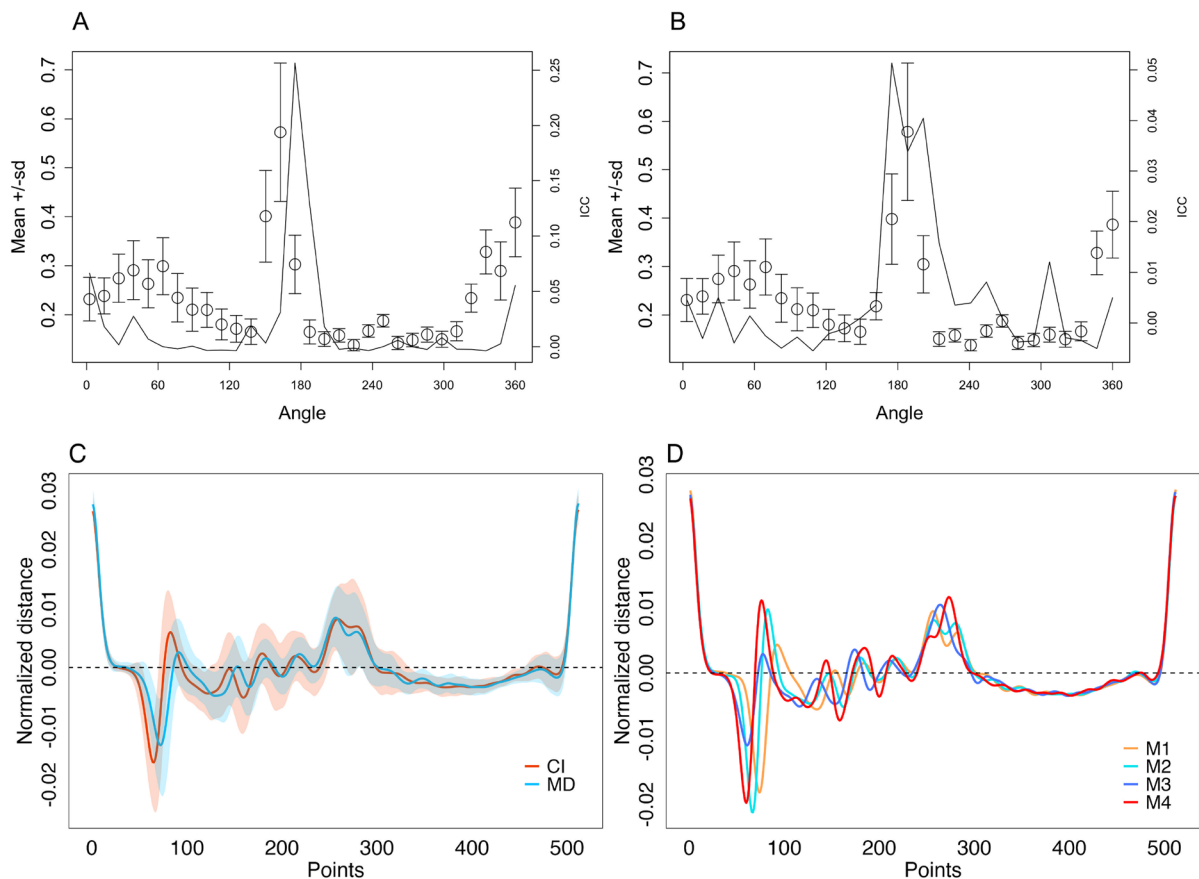


Fig. 2 Mean (open circles) and standard deviation (sd, vertical bars) of the wavelet coefficients obtained from *shapeR* package, standardized for otolith size, for both average phenotype (A) and four morphotypes (M1, M2, M3, and M4) (B). Furthermore, it illustrates the proportion of variance among *Trachurus picturatus* populations (A) and morphotypes (B), sampled from the north and central eastern Atlantic Ocean, specifically from the Canary (CI) and Madeira (MD) archipelagos, represented by the intra-class correlation (ICC, solid line). The horizontal axis is represented in degrees ($^{\circ}$) based

on polar coordinates, with the centroid of the otolith serving as the central point of the polar coordinates. Mean (solid line) and standard deviation (shading) of otolith contour decomposition, using wavelet coefficients obtained through the AFORO protocol in R, for the average phenotype (C) and four morphotypes (M1, M2, M3 and M4) (D). It highlights regions with higher intraspecific variability. The X-axis represents the 512 equidistant points along the perimeter, while Y-axis represents the mean normalized distance

Table S3). This distribution of variance across multiple PCs is characteristic of the complex and nuanced nature of otolith shape data. Specifically, the PC1 axis (which contributed 8.44% of the total variance) enabled the distinction between the CI and MD populations (Fig. 3C). Such a spread of variance, characterized by numerous subtle variations contributing to overall morphology, was evident in our study of biological shapes. The overall average wavelet shape showed intra- and inter-population variability in the *rostrum*, *antirostrum*, dorsal and posterior-ventral regions (Fig. 2C). Particularly,

the MD population displayed a smaller *rostrum* and *antirostrum* region and a wider *excissura ostii* compared to the CI population (Fig. 2C). The PERMANOVA analysis indicated a clear regional differentiation ($F = 28.59$, $p = 0.001$).

Accuracy of classification

Among the four selected classifiers, the Multilayer Perceptron (MLP) and Support Vector Machine (SVM) classifiers exhibited the highest accuracy and Cohen's kappa index (κ) values for both the *shapeR*

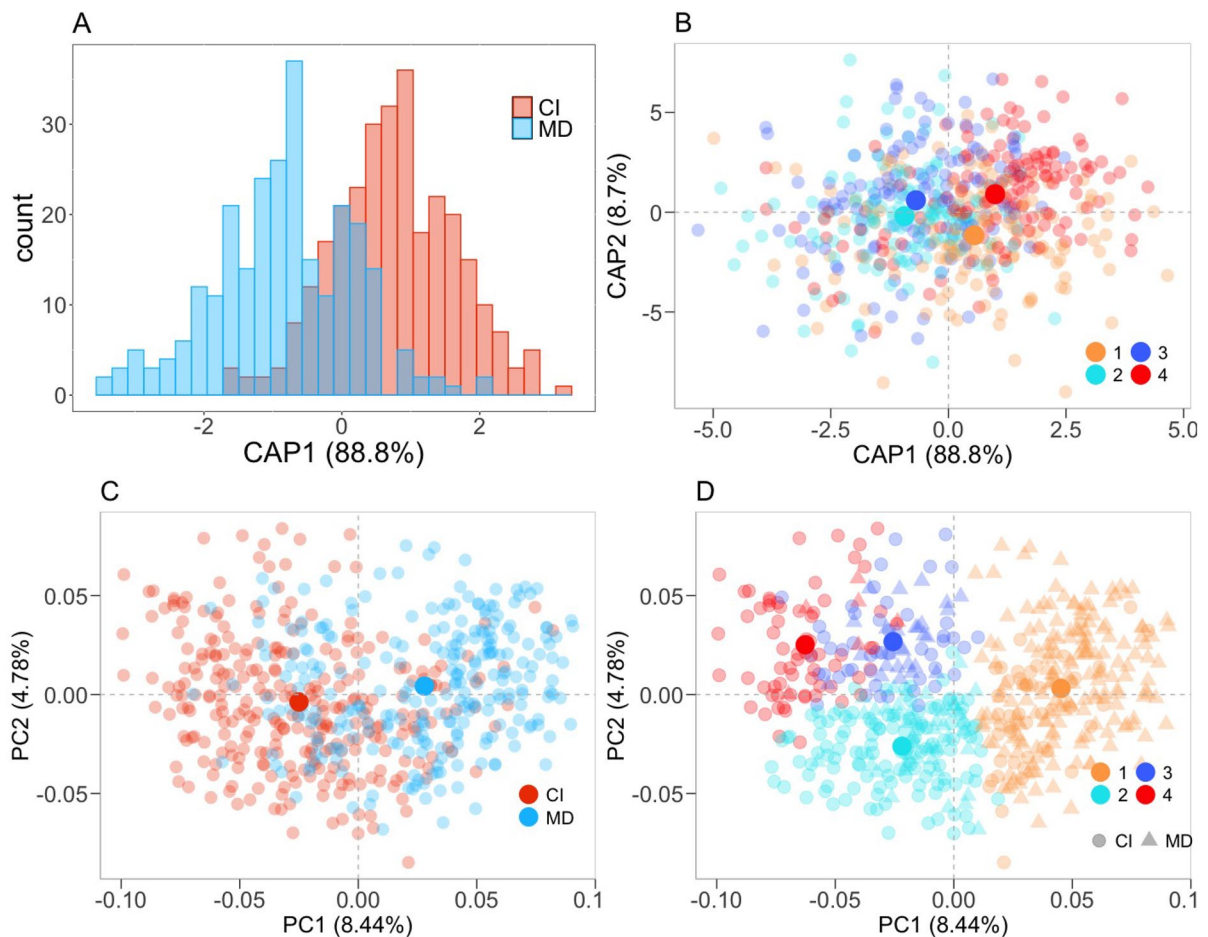


Fig. 3 First discriminating axis (CAP1) of the Canonical analysis of Principal Coordinates (CAP) for the average phenotype (A), along with a scatterplot of the first and second CAP for four morphotypes (M1, M2, M3, and M4) (B) using wavelets coefficients obtained through *shapeR*. This analysis used standardized wavelet coefficients adjusted for otolith size from two populations of *Trachurus picturatus* sampled from the north and central eastern Atlantic Ocean, specifically from

the Canary (CI) and Madeira (MD) archipelagos. The solid-colored circles represent the mean canonical for each morphotype (centroids). Additionally, scatterplots of the first and second axes of the Principal Component Analysis alongside marginal density distribution plots for average phenotype (C) and the four otolith morphotypes (M1, M2, M3 and M4) (D), using wavelet coefficients obtained through the AFORO protocol in R

(Supplementary Table S2) and the AFORO methods (Supplementary Table S4).

For *shapeR* method, when considering the best classifier option (MLP), the classification accuracy for regional populations was found to be 98.55% (Table 1), and the Cohen's kappa index was 0.971, indicating that the classification efficiency was 97% better than what would be expected by chance alone (Table 1). The relative importance of individual wavelet coefficients was consistent among classifiers

revealing a higher importance of those related to low level of pyramidal analysis (e.g., 11, 12 and 4) (Supplementary Figure 5A).

For the AFORO method, when considering the best classifier option (MLP), the classification accuracy for regional populations was found to be 99.82%, and κ was 0.996, indicating that the classification efficiency was 99% better than what would be expected by chance alone (Table 1). The accuracy was particularly high for both CI (100%) and MD (99.62%)

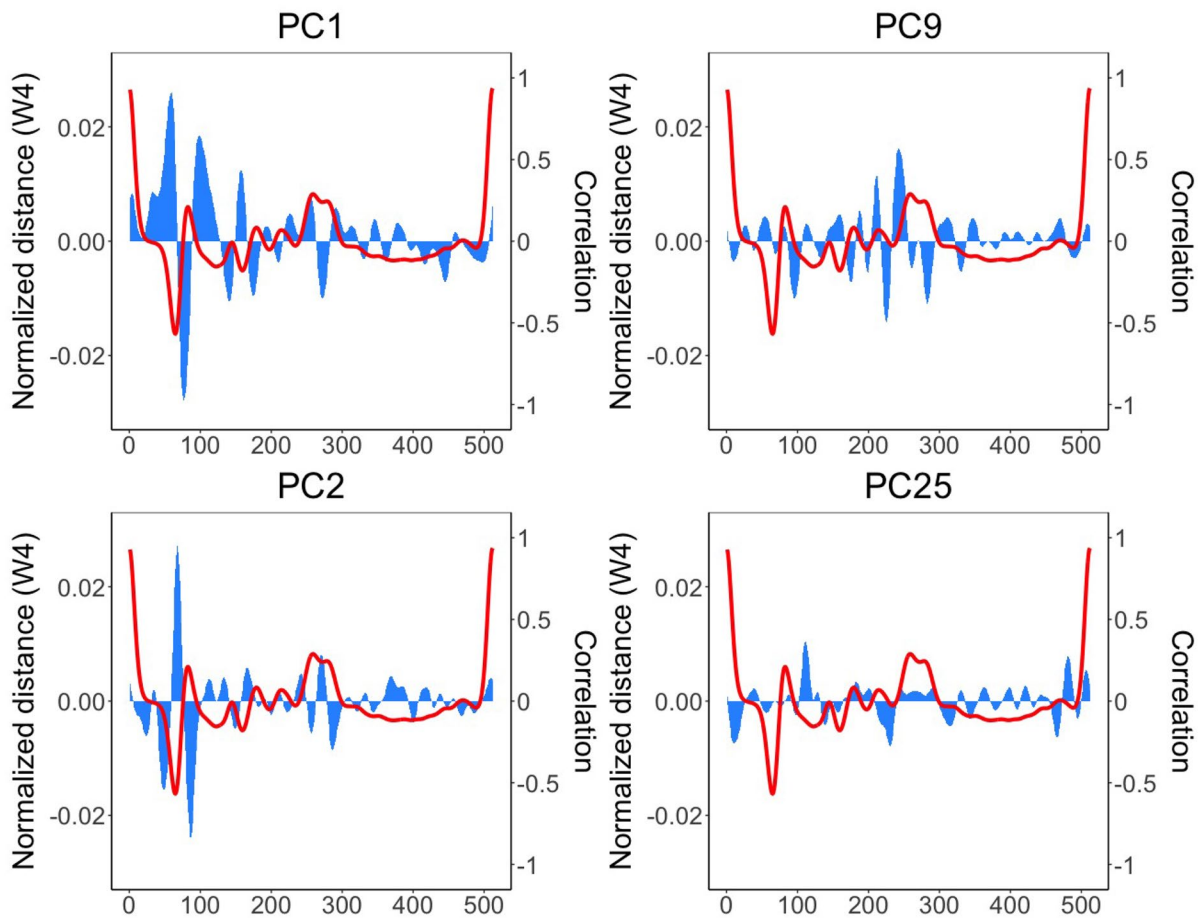


Fig. 4 Correlation of the most relevant principal components (PC) for classification with normalized distance of the 4th wavelet for *Trachurus picturatus* sampled from the north and

central eastern Atlantic Ocean, specifically from the Canary (CI) and Madeira (MD) archipelagos. This analysis employed wavelet coefficients obtained using the AFORO protocol in R

populations. The relative importance of PC components was consistent among statistical classifiers, with PC1 being the most relevant (Supplementary Figure 5B). Specifically, PC1 was highly correlated with the *notch* depth and size of the *antirostrum*, while PC9 was associated with the posterior region (Fig. 4).

Our analysis revealed a substantial agreement between the predictions generated by the AFORO and *shapeR* methods, with an overall agreement rate of approximately 98% (Table 2). Specifically, the models demonstrated a high level of concordance in predicting ‘CI’ outcomes, with agreement rates exceeding 98%, while also displaying notable consistency in predicting ‘MD’ outcomes, with agreement rates surpassing 98%.

Identifying and comparing phenotypes

The Self-Organizing Tree Algorithm (SOTA), known for its efficiency and suitability for clustering a large number of objects, emerged as the most robust method for validating the identification of four phenotypes (M1-4) in both the *shapeR* and the AFORO protocol in R.

Applying the SOTA method and subsequent analysis of the four phenotypes obtained using the *shapeR* method revealed variations among populations in average otolith contours (Figs. 1B and 2B). The intra-class correlation (ICC) and the mean and standard deviation (Fig. 2B) was higher between angles 160–220°, corresponding to the *rostrum* peak and ventral margin. Another secondary zone exhibited small

Fig. 5 Variation of each morphotype of *Trachurus picturatus* sampled from the north and central eastern Atlantic Ocean, specifically from the Canary (CI) and Madeira (MD) archipelagos using wavelet coefficients obtained from *shapeR* (A) and from AFORO protocol in R (B). This graph aims to demonstrate that each phenotype undergoes changes in each region, likely influenced by environmental conditions such as temperature, as previously observed by Vasconcelos et al. (2021)

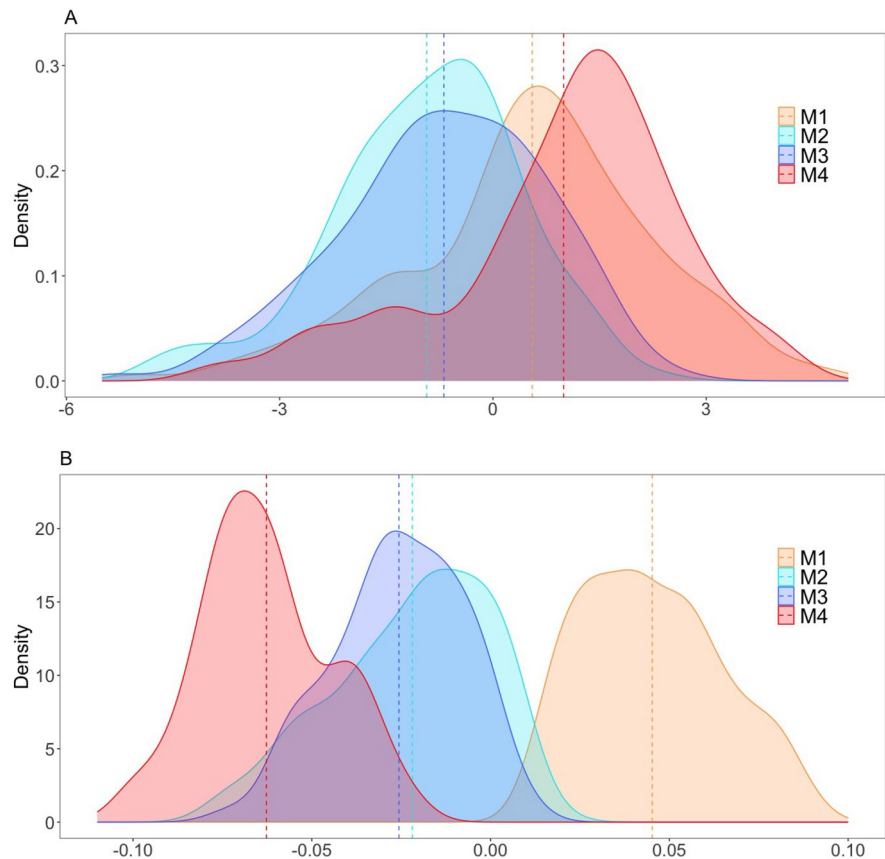


Table 1 Abundances and classification accuracy of individuals to their sampling origin, detailing the assignment percentage of each actual group membership with its correct predicted group highlighted in bold. This analysis is based on the population variation at two locations in the north and central eastern Atlantic Ocean, specifically the Canary (CI) and Madeira

(MD) archipelagos. The non-parametric classification algorithm Multilevel Perceptron (MLP) was employed, using wavelets obtained from both the *shapeR* R package and the AFORO protocol in R. Wavelets were standardized for otolith (OL) lengths

R package	Prediction	References		Performance measures		
		CI	MD	Accuracy	Kappa	% Accuracy
<i>shapeR</i>	CI	286	4	0.986	0.971	98.62
	MD	4	256			98.46
	Total	290	260			
AFORO	CI	290	1	0.998	0.996	100
	MD	0	259			99.62
	Total	290	260			

variations around 320° (posterior ventral margin). Significant differences were found between morphotypes (ANOVA: pseudo-F= 12.23, df = 3, $p = 0.001$), although with a high degree of overlapping in the spatial distribution (Fig. 3B). When applying

the Kruskal-Wallis test, the median value of CAP1 also indicated significant differences (KW test, $H = 132.33$, $p < 0.05$), except for the comparison between M2 and M3 (WRS test, $p = 0.87$) (Fig. 5A). In the Canary Islands, M4 was the most abundant,

Table 2 Comparison of predictions between *shapeR* and AFORO methods. The rows represent predictions made by the AFORO, while the columns represent predictions made by the *shapeR*. Each cell in the table shows the count of observations that fall into a particular combination of predictions

Predicted AFORO	Predicted <i>shapeR</i>		Total
	CI	MD	
CI	286 98.62%	5 1.92%	291
MD	4 1.38	255 98.08%	259
Total	290 52.73%	260 47.27%	550

accounting for 34.8% of the total individuals analysed. It was closely followed by M1 (33.4%), while M3 (16.6%) and M2 (15.2%) were less common. In contrast, the MD population exhibited different frequencies of morphotypes: M2 was the most common (36.2%), closely followed by M3 (30.8%) and in lesser frequency M1 (19.6%) and M4 (13.5%).

The PCA analysis conducted using wavelets obtained from the AFORO successfully enabled the distinction of all four morphotypes (Fig. 3D). Individuals belonging to morphotype M1 exhibited a more rounded *antirostrum* and a wider *excissura ostii* for positive values of the PC1 axis, which accounted for 8.44% of the total variance (Fig. 3D). Morphotypes M2 and M4 both exhibited a deep *notch* with a peak-shaped *antirostrum*. However, they differed in the posterior region, with M4 having a more lanceolate shape and M2 having a rounder shape. When considering the positive values of the PC2 axis (4.78% of the total variance) the morphotype M3 demonstrated distinct features such as a shallower *notch* and smaller or absent *antirostrum* (Figs. 2D and 3D). In the MD area, the most prevalent morphotypes were M1 (69.2%), followed by M2 (17.7%) and M3 (10.4%), with M4 being scarce (2.3%). In the CI, the most prevalent morphotypes were M2 (44.1%) and M4 (23.1%), with M3 (16.6%) and M1 (16.2%) occurring in similar frequencies. The variability of the first PC component between phenotypes (Fig. 5B), revealed significant differences (KW test, $H = 440.38$, $p < 0.05$), except for the comparison between M2 and M3 (WRS test, $p = 0.56$) (Fig. 5B).

The cross-tabulation analysis comparing morphotypes derived from *shapeR* and AFORO revealed differing proportions across the four morphotype

Table 3 Frequencies and proportions of individuals classified into each category (morphotype) by both *shapeR* and AFORO methods. The rows represent the categories of the AFORO variable (M1-M4), while the columns represent the categories of the *shapeR* variable (M1-M4). The values in the cells indicate the count of observations that belong to the corresponding combination of categories and the proportion of individuals from each method's classification within each population group

Predicted AFORO	Predicted <i>shapeR</i>				Total
	1	2	3	4	
1	57 25.00% 38.51%	70 30.70% 50.73%	65 28.51% 50.78%	36 15.79% 26.47%	228 41.46%
2	54 31.03% 36.49%	35 20.15% 25.36%	28 16.09% 21.88%	57 32.76% 41.91%	174 31.64%
3	19 25.332% 12.84%	19 25.33% 13.77%	24 32.00% 18.75%	13 17.33% 9.56%	75 13.64%
4	18 24.66% 12.16%	14 19.78% 10.15%	11 15.07% 8.59%	30 41.10% 22.06%	73 13.27%
Total	148 26.91%	138 25.09%	128 23.27%	136 24.73%	550

categories (M1, M2, M3, and M4) (Table 3). Given that the distribution of *shapeR* proportions is identical for all four morphotypes, which may not align well with the concept of phenotypic plasticity, the phenotype predictions of AFORO were considered a more realistic basis for comparison between methods (Table 3). For instance, among individuals categorized as group M1 by the AFORO method, only 25.0% were also classified into group M1 by *shapeR*, while the majority (30.7%) of individuals classified into group M1 by the AFORO method were classified into group M2 by the *shapeR* method. The highest level of concordance between methods was found in group M4, with 41.1% ($n=30$) of the individuals classified as group M4 by the AFORO method also classified as M4 by the *shapeR* method.

Discussion

This study has demonstrated the suitability of both the *shapeR* R package and the AFORO protocol in

R for population identification. The effectiveness of the protocols is not solely determined by numerical outcomes; mathematical models should also exhibit a clear and reliable practical application in morphology. Within this framework, the underlying philosophy behind wavelets, from which they originated, is not apparent in the *shapeR* package. It is crucial to highlight that this observation does not discredit the results obtained with this package; instead, it deviates from the approach that, as morphologists, we deem suitable for tackling intricate morphological challenges beyond stock identification. Furthermore, several morphological inconsistencies or challenges were noted when using the *shapeR* package compared to the AFORO protocol.

Limitations of *shapeR*: An examination of weaknesses

There are certain limitations associated with using the *shapeR* package, including: (1) The requirement for precise horizontal alignment of otolith positions in photographs, as the initial point is not anchored to an anatomical structure such as the *rostrum*. This issue could be addressed by calculating the centroid of the otolith shape and defining the initial point as the maximum distance to the rightward-facing *rostrum*. As a result, perfect alignment of images may not be necessary; (2) The otolith mean shape obtained from the function *plotWaveletShape* does not maintain the aspect ratio of the plot. When the aspect ratio parameter (*asp*=1) is added, all other elements of the plot (such as the degrees) disappear except for the mean contour. This problem is evident in various publications (e.g., Rodgveller et al. 2017; Christensen et al. 2018; Mahé et al. 2019; Osman et al. 2021; Wujdi et al. 2022; Deville et al. 2023; Muñoz-Lechuga et al. 2023) where the mean shapes depicted do not accurately reflect the true otolith morphology. From a morphological perspective, attempting comparisons between studies on the same fish taxa becomes problematic when there is inconsistency in the standardization of images; (3) Establishing a connection between the average otolith shape (Fig. 1) and the intraclass correlation (ICC) plots (Fig. 2A and B). In the *shapeR* it is not evident which points (degrees) of the contour are correlated to the ICC and to the number of selected coefficients. Moreover, the morphological interpretation of ICC as the area with the

greatest disparities between populations is subject to question in numerous studies. Even when such a plot is not provided, authors often ascertain differences using the sole criterion of mean shape (e.g., Morawicki et al. 2022; Morales et al. 2023; Park et al. 2023; Vaz et al. 2023). Although the mean contour consistently captures attention and offers valuable insights, the standard deviation plays a critical role in elucidating the precise locations of morphological variability. Additionally, it would be beneficial to identify regions with significant differences, a task that is not feasible through these plots alone.

Similarities and disparities between methods

The only similarity found between both methods was the high success rate in classifying individuals to their respective population samples (population identification). The non-parametric classification algorithm Multi-Level Perceptron (MLP) emerged as the top performer, yielding robust results for both protocols (Table 1). This highlights that both methods are viable options. Contrarily, several disparities emerged between the methodologies, namely: (1) The *shapeR* package collects only polar coordinates, whereas the AFORO protocol offers both polar and Cartesian coordinates; (2) The *shapeR* package lacks a linkage between the starting point of the contour shape analysis and a morphological feature, whereas in the AFORO protocol, an algorithm detects the point on the *rostrum* furthest from the centroid; (3) While *shapeR* consistently recommends the 5th level as the optimal choice (e.g., Deville et al. 2023,), AFORO provides researchers with the flexibility to select the appropriate wavelet level based on the study type and the morphological intricacies of the otolith contour. With *shapeR*, certain otoliths displaying high irregularity may appear smoother, leading to the loss of crucial information. Moreover, the AFORO representation of wavelets seems to offer greater clarity and ease of interpretation. One advantage of this visualization approach is its capability to facilitate morphological comparisons across species, as demonstrated in the AFORO web platform, where all images undergo morphological standardization (Lombarte et al. 2006), or stocks (Sadighzadeh et al. 2014; Tuset et al. 2019; Vasconcelos et al. 2021); (4) In *shapeR*, wavelet coefficients that exhibit a significant interaction with otolith size can be eliminated, while

in AFORO, they are retained, and their influence is managed through the use of residuals obtained from the common within-group slopes observed in the linear regressions of each principal component against otolith size; (5) There is no correlation between ICC and the discriminating axis of the CAP in *shapeR*, whereas in AFORO, there is a correlation of the most relevant PC components from the discriminant analysis (Fig. 4), with specific zones of the otolith contour. From *shapeR*, we can only obtain information regarding which coefficients are the most important, but we cannot correlate them with any specific zone of the otolith.

Another notable dissimilarity observed relates to the determination of phenotypes. When assessing the number and abundance of each morphotype within the entire sample, the AFORO protocol suggests an ecological interpretation more aligned with reaction norms, which is defined as the 'phenotypic expression of a genotype in different environments' (Schmalhausen 1949; Pigliucci 2001; West-Eberhard 2003; Donohue 2016). This plasticity was evident in our study, where varying proportions of morphotypes in the Canary and Madeira regions reflect a shift towards new optimal phenotypes in response to distinct environmental conditions. Among the exogenous factors influencing these adaptations, temperature gradients, particularly SST, appear to play a crucial role (O'Dea et al. 2019). For instance, in Madeira, morphotype M1 predominates, potentially reflecting local environmental preferences. In contrast, in the Canaries, where SST may be higher, we observe higher frequencies of morphotypes like M3 and M4, which are less prevalent in Madeira. However, for *shapeR*, this variation in the proportion of morphotypes per region does not seem to have an ecological meaning coherent with reaction norms. While the SOTA clustering algorithm identified four morphotypes using both methods, a significant disparity arose in the individual assignments to each morphotype in *shapeR* (Table 3), with a similar frequency of individual assignments among the four identified morphotypes (M1: 148, M2: 138, M3: 128, and M4: 136). It does not seem plausible for the relative abundance of phenotypes to remain constant across different environmental conditions and not follow a reaction norm.

From this analysis, it appears that *shapeR* may not be adequately equipped for intraspecies studies. The flexibility of selecting the wavelet level in

AFORO makes this method more appealing. For instance, AFORO's use of the 4th wavelet level proves more conducive to identifying intraspecific phenotypes (Tuset et al. 2019; Vasconcelos et al. 2021), as it requires a higher level of detail. This capability proves particularly beneficial in delineating stock boundaries and analyzing species adaptability to climate change.

Conclusion

Since the introduction of the *shapeR* package, many studies have adopted this methodology for analyzing otolith contour shapes (Vaux et al. 2019; Neves et al. 2021; Deville et al. 2023; Neves et al. 2023; Park et al. 2023; Neves et al. 2024). While their interpretations and conclusions may indeed be valid, doubts persist regarding the morphology. Numerical outcomes, such as classification success, do not solely serve as the most crucial results, with morphological disparities among populations potentially holding greater ecological relevance. We propose a review of the identified issues within the *shapeR* package from a user's perspective.

Acknowledgements Fish samples from Madeira were provided by the Regional Directorate of Fisheries (DRP), and from the Canary Islands (Spain) by the Canary Oceanographic Centre of the Spanish Oceanographic Institute (IEO). Authors would like to thank all the colleagues who participated in the samples collection and fish biological samplings.

Author contributions Joana Vasconcelos: Conceptualization, Biological sampling, Data acquisition, Data curation, Methodology, Formal analysis and investigation, Statistical analysis, Validation, Critical analysis, Writing—Original draft preparation, Writing—review and editing. José Luís Otero-Ferrer: Software, Statistical analysis, Writing—review and editing. Antoni Lombarte: Data interpretation, Critical analysis, Validation, Writing—review and editing. Alba Jurado-Ruzafa: Biological sampling, Data acquisition, Data curation, Writing—review and editing. Amalia Manjabacas: Software, Validation, Writing—review and editing. Victor M. Tuset: Conceptualization, Data interpretation, Critical analysis, Supervision, Writing—Original draft, Writing—review and editing.

Funding The first author (JV) was supported by the 'Grants for the Viera y Clavijo training program for researchers' of the Government of the Canary Islands (VIERA Y CLAVIJO-2022-CIENCIAS-1). This research was also funded by the Portuguese national funds through Fundação para a Ciência e a Tecnologia I.P. (FCT) in the framework of MARE grant number UIDB/04292/2020 and Associate Laboratory ARNET

grant number LA/P/0069/2020, the National Data Collection Framework, and the University of Las Palmas of Gran Canaria (ULPGC).

Data availability The datasets generated during and/or analysed during the current study are available from the corresponding author on reasonable request.

Declarations

Conflict of interest JO-F was employed by Biostatech, Advice, Training & Innovation in Biostatistics, S.L. The remaining authors have no Conflict of interest to declare that are relevant to the content of this article.

Open Access This article is licensed under a Creative Commons Attribution-NonCommercial-NoDerivatives 4.0 International License, which permits any non-commercial use, sharing, distribution and reproduction in any medium or format, as long as you give appropriate credit to the original author(s) and the source, provide a link to the Creative Commons licence, and indicate if you modified the licensed material. You do not have permission under this licence to share adapted material derived from this article or parts of it. The images or other third party material in this article are included in the article's Creative Commons licence, unless indicated otherwise in a credit line to the material. If material is not included in the article's Creative Commons licence and your intended use is not permitted by statutory regulation or exceeds the permitted use, you will need to obtain permission directly from the copyright holder. To view a copy of this licence, visit <http://creativecommons.org/licenses/by-nc-nd/4.0/>.

References

- Abaunza P, Murta A, Campbell N, Cimmaruta R, Comesaña A, Dahle G, Santamaría MG, Gordo L, Iversen S, MacKenzie K (2008) Stock identity of horse mackerel (*Trachurus trachurus*) in the northeast atlantic and mediterranean sea: integrating the results from different stock identification approaches. *Fish Res* 89(2):196–209. <https://doi.org/10.1016/j.fishres.2007.09.022>
- Anderson MJ, Willis TJ (2003) Canonical analysis of principal coordinates: a useful method of constrained ordination for ecology. *Ecology* 84(2):511–525
- Anderson MJ (2001) A new method for non-parametric multivariate analysis of variance. *Austral Ecol* 26(1):32–46. <https://doi.org/10.1111/j.1442-9993.2001.01070.pp.x>
- Begg GA, Campana SE, Fowler AJ, Suthers IM (2005) Otolith research and application: current directions in innovation and implementation. *Mar Freshw Res* 56(5):477–483. <https://doi.org/10.1071/MF05111>
- Begg GA, Friedland KD, Pearce JB (1999) Stock identification and its role in stock assessment and fisheries management: an overview. *Fish Res* 43(1–3):1–8
- Bird JL, Eppler DT, Checkley DM Jr (1986) Comparisons of herring otoliths using fourier series shape analysis. *Can J Fish Aquat Sci* 43(6):1228–1234
- Brock G, Pihur V, Datta S, Datta S (2008) clvalid: An r package for cluster validation. *J Stat Softw* 25:1–22
- Burke N, Brophy D, King PA (2008) Otolith shape analysis: its application for discriminating between stocks of irish sea and celtic sea herring (*Clupea harengus*) in the irish sea. *ICES J Mar Sci* 65(9):1670–1675
- Cadrin SX, Kerr LA, Mariani S (2013) Stock identification methods: applications in fishery science. Elsevier
- Campana SE, Casselman JM (1993) Stock discrimination using otolith shape analysis. *Can J Fish Aquat Sci* 50(5):1062–1083. <https://doi.org/10.1139/f93-123>
- Christensen HT, Rigét F, Backe MB, Saha A, Johansen T, Hedeholm RB (2018) Comparison of three methods for identification of redfish (*Sebastes mentella* and *S. norvegicus*) from the greenland east coast. *Fish Res* 201:11–17
- Deville D, Kawai K, Fujita H, Umino T (2023) Ecomorphology of three closely related *Sebastes* rockfishes with sympatric occurrence in seto inland sea, japan. *Hydrobiologia*, 1–18. <https://doi.org/10.1007/s10750-023-05286-4>
- Donohue K (2016) Genotype-by-environment interaction. In: Kliman, R.M. (ed.) *Encyclopedia of Evolutionary Biology*, pp. 186–194. Academic Press, Oxford. <https://doi.org/10.1016/B978-0-12-800049-6.00049-4>. <https://www.sciencedirect.com/science/article/pii/B978012800049600494>
- Friedland K, Reddin D (1994) Use of otolith morphology in stock discriminations of atlantic salmon (*Salmo salar*). *Can J Fish Aquat Sci* 51(1):91–98
- Gauldie R, Crampton J (2002) An eco-morphological explanation of individual variability in the shape of the fish otolith: comparison of the otolith of *Hoplostethus atlanticus* with other species by depth. *J Fish Biol* 60(5):1204–1221. <https://doi.org/10.1111/j.1095-8649.2002.tb01715.x>
- Gençay R, Selçuk F, Whitcher B (2001) Differentiating intraday seasonalities through wavelet multi-scaling. *Physica A* 289(3–4):543–556
- Harbitz A, Albert OT (2015) Pitfalls in stock discrimination by shape analysis of otolith contours. *ICES J Mar Sci* 72(7):2090–2097. <https://doi.org/10.1093/icesjms/fsv048>
- Hills J, Lines J, Baranaukas E, Mapp J, Bagnall A (2014) Classification of time series by shapelet transformation. *Data Min Knowl Disc* 28:851–881
- Jurado-Ruzafa A, García Santamaría M (2013) Reproductive biology of the blue jack mackerel, *Trachurus picturatus* (Bowdich, 1825), off the canary islands. *J Appl Ichthyol* 29(3):526–531. <https://doi.org/10.1111/jai.12049>
- Jónsson EP, Campana SE, Sólmundsson J, Jakobsdóttir KB, Bárðarson H (2021) The effect of growth rate on otolith-based discrimination of cod (*Gadus morhua*) ecotypes. *PLoS ONE* 16(9):0247630
- Kuhl FP, Giardina CR (1982) Elliptic fourier features of a closed contour. *Comput Graph Image Process* 18(3):236–258
- Kuhn M (2008) Building predictive models in r using the caret package. *Journal of statistical software* 28, 1–26 <https://doi.org/10.18637/jss.v028.i055>
- Kumar P, Foufoula-Georgiou E (1994) Wavelet analysis in geophysics: an introduction. *Wavelets Geophys* 4:1–43
- Kutskir I (2022) Photopea (Version 5.4) [Computer software]. Retrieved from <https://www.photopea.com/>

- Libungan LA, Pálsson S (2015) Shaper: an R package to study otolith shape variation among fish populations. *PLoS ONE* 10(3):0121102. <https://doi.org/10.1371/journal.pone.0121102>
- Libungan L, Óskarsson G, Slotte A, Jacobsen J, Pálsson S (2015) Otolith shape: a population marker for atlantic herring *Clupea harengus*. *J Fish Biol* 86(4):1377–1395
- Libungan LA, Pálsson S (2022) ShapeR: collection and analysis of Otolith shape data, R package version 0.1-5
- Lines J, Davis LM, Hills J, Bagnall A (2012) A shapelet transform for time series classification. In: *Proceedings of the 18th ACM SIGKDD International Conference on Knowledge Discovery and Data Mining*, pp. 289–297
- Lombarte A, Castellón A (1991) Interspecific and intraspecific otolith variability in the genus *Merluccius* as determined by image analysis. *Can J Zool* 69(9):2442–2449
- Lombarte A, Chic Ó, Parisi-Baradad V, Olivella R, Piera J, García-Ladona E (2006) A web-based environment for shape analysis of fish otoliths. the AFORO database. *Sci Marina* 70:147–152
- Lombarte A, Miletic M, Kovačić M, Otero-Ferrer JL, Tuset VM (2018) Identifying sagittal otoliths of mediterranean sea gobies: variability among phylogenetic lineages. *J Fish Biol* 92(6):1768–1787
- Lombarte A, Morales-Nin B (1995) Morphology and ultrastructure of saccular otoliths from five species of the genus *Coelorrinchus* (gadiformes: Macrouridae) from the south-east Atlantic. *J Morphol* 225(2):179–192
- Mahé K, Gourtay C, Defruit GB, Chantre C, Pontual H, Amara R, Claireaux G, Audet C, Zambonino-Infante J-L, Ernande B (2019) Do environmental conditions (temperature and food composition) affect otolith shape during fish early-juvenile phase? an experimental approach applied to european seabass (*Dicentrarchus labrax*). *J Exp Mar Biol Ecol* 521:151239
- Mapp J, Fisher M, Bagnall T, Lines J, Songer S, Scutt Phillips J (2013) *Clupea harengus*: Intraspecific distinction using curvature scale space and shapelets. In: *Proc. 2nd International Conference on Pattern Recognition Applications and Methods, ICPRAM*
- Marengo M, Baudouin M, Viret A, Laporte M, Berrebi P, Vignon M, Marchand B, Durieux E (2017) Combining microsatellite, otolith shape and parasites community analyses as a holistic approach to assess population structure of *Dentex dentex*. *J Sea Res* 128:1–14
- Messieh SN, MacDougall C, Claytor R (1989) Separation of Atlantic herring (*Clupea harengus*) stocks in the southern gulf of St. Lawrence using digitized otolith morphometrics and discriminant function analysis. *Can Tech Rep Fish Aquat Sci* 1647:1–22
- Morales CJC, Barnuevo KDE, Delloro ES Jr, Cabebe-Barnuevo RA, Calizo JKS, Lumayno SDP, Babaran RP (2023) Otolith morphometric and shape distinction of three redfin species under the genus *Decapterus* (teleostei: Carangidae) from sulu sea, Philippines. *Fishes* 8(2):95
- Morawicki S, Solimano PJ, Volpedo AV (2022) Unravelling stock spatial structure of silverside *Odontesthes argentinensis* (valenciennes, 1835) from the north argentinian coast by otoliths shape analysis. *Fishes* 7(4):155. <https://doi.org/10.3390/fishes7040155>
- Muñoz-Lechuga R, Sow FN, Constance DN, Angueko D, Macías D, Massa-Gallucci A, Silva GB, Gonçalves JM, Lino PG (2023) Differentiation of spatial units of genus *Euthynnus* from the eastern atlantic and the mediterranean using otolith shape analysis. *Fishes* 8(6):317
- Nason G (2012) wavethresh: Wavelets statistics and transforms, version 4.5. R package. <http://CRAN.R-project.org/package=wavethresh>
- Nasreddine K, Benzinou A, Fablet R (2009) Shape geodesics for the classification of calcified structures: beyond fourier shape descriptors. *Fish Res* 98(1–3):8–15. <https://doi.org/10.1016/j.fishres.2009.03.008>
- Neves J, Silva AA, Moreno A, Verissimo A, Santos AM, Garrido S (2021) Population structure of the european sardine *Sardina pilchardus* from atlantic and mediterranean waters based on otolith shape analysis. *Fish Res* 243:106050
- Neves J, Verissimo A, Múrias Santos A, Garrido S (2023) Comparing otolith shape descriptors for population structure inferences in a small pelagic fish, the european sardine *Sardina pilchardus* (walbaum, 1792). *J Fish Biol* 102(5):1219–1236
- Neves J, Verissimo A, Santos AM, Garrido S (2024) Age affects otolith shape in a coastal pelagic fish (*Scomber colias* Gmelin, 1789). *Fish Res* 270:106881
- Oksanen J, Simpson G, Blanchet F, Kindt R, Legendre P, Minchin P, O'Hara R, Solymos P, Stevens M, Szoecs E et al (2022) *Vegan: Community ecology package* (R package version 2.6-4)
- Osman YA, Pálsson S, Makkey AF (2021) Otolith shape analysis of *Lethrinus lentjan* (lacepède, 1802) and *L. microdon* (valenciennes, 1830) from the red sea. *Int J Aquat Biol* 9(3):159–166
- O'Dea RE, Lagisz M, Hendry AP, Nakagawa S (2019) Developmental temperature affects phenotypic means and variability: A meta-analysis of fish data. *Fish Fish* 20(5):1005–1022
- Parisi-Baradad V, Lombarte A, García-Ladona E, Cabestany J, Piera J, Chic O (2005) Otolith shape contour analysis using affine transformation invariant wavelet transforms and curvature scale space representation. *Mar Freshw Res* 56(5):795–804
- Parisi-Baradad V, Manjabacas A, Lombarte A, Olivella R, Chic Ó, Piera J, García-Ladona E (2010) Automated taxon identification of teleost fishes using an otolith online database. *Fish Res* 105(1):13–20
- Park JM, Kang MG, Kim JH, Jawad LA, Majeed S (2023) Otolith morphology as a tool for stock discrimination of three rockfish species in the east sea of korea. *Front Mar Sci* 110:1301178. <https://doi.org/10.3389/fmars.2023.1301178>
- Piera J, Parisi-Baradad V, García-Ladona E, Lombarte A, Recasens L, Cabestany J (2005) Otolith shape feature extraction oriented to automatic classification with open distributed data. *Mar Freshw Res* 56(5):805–814
- Pigliucci M (2001) *Phenotypic Plasticity: Beyond Nature and Nurture*. The John Hopkins University Press, Baltimore
- R Core Team (2023) *R: A Language and Environment for Statistical Computing*. R Foundation for Statistical Computing, Vienna, Austria. R Foundation for Statistical Computing. <https://www.R-project.org/>

- Rodgveller CJ, Hutchinson CE, Harris JP, Vulstek SC, Guthrie CM III (2017) Otolith shape variability and associated body growth differences in giant grenadier, *Albatrossia pectoralis*. PLoS One 12(6):0180020
- Sadeghi R, Esmaili HR, Zarei F, Reichenbacher B (2020) Population structure of the ornate goby, *Istigobius ornatus* (teleostei: Gobiidae), in the persian gulf and oman sea as determined by otolith shape variation using shaper. Environ Biol Fishes 103:1217–1230
- Sadighzadeh Z, Tuset VM, Valinassab T, Dadpour MR, Lombarte A (2012) Comparison of different otolith shape descriptors and morphometrics for the identification of closely related species of *Lutjanus* spp. from the persian gulf. Marine Biol Res 8(9):802–814
- Sadighzadeh Z, Valinassab T, Vosugi G, Motallebi A, Fatemi MR, Lombarte A, Tuset VM (2014) Use of otolith shape for stock identification of john's snapper, *Lutjanus johnii* (pisces: Lutjanidae), from the persian gulf and the oman sea. Fish Res 155:59–63
- Schmalhausen II (1949) Factors of Evolution. The Theory of Stabilizing Selection. Blakiston, Philadelphia, 326.
- Schneider CA, Rasband WS, Eliceiri KW (2012) Nih image to imagej: 25 years of image analysis. Nat Methods 9(7):671–675
- Schroeder R, Schwingel PR, Correia AT (2022) Population structure of the brazilian sardine (*Sardinella brasiliensis*) in the southwest atlantic inferred from body morphology and otolith shape signatures. Hydrobiologia 849(6):1367–1381
- Smoliński S, Schade FM, Berg F (2020) Assessing the performance of statistical classifiers to discriminate fish stocks using fourier analysis of otolith shape. Can J Fish Aquat Sci 77(4):674–683
- Soeth M, Spach HL, Daros FA, Adelir-Alves J, Almeida ACO, Correia AT (2019) Stock structure of Atlantic spadefish *Chaetodipterus faber* from southwest Atlantic Ocean inferred from otolith elemental and shape signatures. Fish Res 211:81–90
- Stransky C, MacLellan SE (2005) Species separation and zoogeography of redbfish and rockfish (genus *Sebastes*) by otolith shape analysis. Can J Fish Aquat Sci 62(10):2265–2276. <https://doi.org/10.1139/f05-143>
- Stransky C, Murta AG, Schlickeisen J, Zimmermann C (2008) Otolith shape analysis as a tool for stock separation of horse mackerel (*Trachurus trachurus*) in the northeast atlantic and mediterranean. Fish Res 89(2):159–166
- Tracey SR, Lyle JM, Duhamel G (2006) Application of elliptical fourier analysis of otolith form as a tool for stock identification. Fish Res 77(2):138–147
- Tuset VM, Imondi R, Aguado G, Otero-Ferrer JL, Santschi L, Lombarte A, Love M (2015) Otolith patterns of rockfishes from the northeastern Pacific. J Morphol 276(4):458–469
- Tuset VM, Jurado-Ruzafa A, Otero-Ferrer JL, Santamaría MTG (2019) Otolith phenotypic variability of the blue jack mackerel, *Trachurus picturatus*, from the canary islands (NE atlantic): Implications in its population dynamic. Fish Res 218:48–58
- Tuset VM, Lombarte A, Assis CA (2008) Otolith atlas for the western mediterranean, north and central eastern atlantic. Sci Mar 72(S1):7–198. <https://doi.org/10.3989/scimar.2008.72s17>
- Tuset VM, Lombarte A, González JA, Pertusa J, Lorente M (2003) Comparative morphology of the sagittal otolith in *Serranus* spp. J Fish Biol 63(6):1491–1504
- Tuset VM, Otero-Ferrer JL, Siliprandi C, Manjabacas A, Marti-Puig P, Lombarte A (2021) Paradox of otolith shape indices: routine but overestimated use. Can J Fish Aquat Sci 78(6):681–692
- Vasconcelos J, Vieira AR, Sequeira V, González JA, Kaufmann M, Gordo LS (2018) Identifying populations of the blue jack mackerel (*Trachurus picturatus*) in the northeast atlantic by using geometric morphometrics and otolith shape analysis. Fish Bull 116:81–92. <https://doi.org/10.7755/FB.116.1.9>
- Vasconcelos J, Jurado-Ruzafa A, Otero-Ferrer JL, Lombarte A, Riera R, Tuset VM (2021) Thinking of fish population discrimination: population average phenotype vs. population phenotypes. Frontiers Marine Sci 8:740296. <https://doi.org/10.3389/fmars.2021.740296>
- Vaux F, Rasmuson LK, Kautzi LA, Rankin PS, Blume MT, Lawrence KA, Bohn S, O'Malley KG (2019) Sex matters: Otolith shape and genomic variation in deacon rockfish (*Sebastes diaconus*). Ecol Evol 9(23):13153–13173
- Vaz A, Guerreiro MA, Landa J, Hannipoula O, Thasitis I, Scarcella G, Sabatini L, Vitale S, Mugerza E, Mahé K (2023) Otolith shape analysis as a tool for stock identification of two commercially important marine fishes: *Helicolenus dactylopterus* and *Merluccius merluccius*. Estuar Coast Shelf Sci 293:108471
- West-Eberhard MJ (2003) Developmental plasticity and evolution. Oxford University Press, Oxford. <https://doi.org/10.1093/oso/9780195122343.001.0001>
- Wujdi A, Kim HJ, Oh CW (2022) Population structure of indian mackerel (*Rastrelliger kanagurta*) in java and bali island, indonesia inferred from otolith shape. Sains Malays 51(1):39–50
- Youssef EH, Youssef E-S, Mostafa MEY, Driss Fathallah CN, Alain (2016) Recognition of otoliths having a high shape similarity. J Theor Appl Inf Tech 84:1923

Publisher's Note Springer Nature remains neutral with regard to jurisdictional claims in published maps and institutional affiliations.